

A solid-state platform for cooperative quantum phenomena

Xin Li,^{1,*} Jamir Marino,² Darrick E. Chang,^{3,4} and Benedetta Flebus¹

¹*Department of Physics, Boston College, 140 Commonwealth Avenue, Chestnut Hill, Massachusetts 02467, USA*

²*Institut für Physik, Johannes Gutenberg-Universität Mainz, D-55099 Mainz, Deutschland*

³*ICFO-Institut de Ciències Fotoniques, The Barcelona Institute of Science and Technology, 08860 Castelldefels (Barcelona), Spain*

⁴*ICREA-Institució Catalana de Recerca i Estudis Avançats, 08010 Barcelona, Spain*

The dissipation resulting from the coupling of a system with its environment is commonly viewed as a foe for quantum technologies. Nonetheless, recent developments at light-matter interfaces have shown that correlated dissipation can be leveraged to engineer novel dynamical states of matter and entanglement in many-body quantum systems. Inspired by this progress, here we set the stage for the – yet uncharted – exploration of cooperative quantum phenomena in quantum hybrid solid-state platforms. We develop a comprehensive formalism for the quantum many-body dynamics of an ensemble of solid-state spin defects interacting via the magnetic field fluctuations of a common solid-state reservoir. Our general framework captures effective qubit-qubit interactions mediated by correlated dissipation and naturally extends the theory of quantum sensing of local magnetic noise via single solid-state spin defects to sensing of nonlocal temporal and spatial correlations. To understand whether dissipative correlations can play a relevant role in a realistic experimental setup, we apply our model to a qubit array interacting via the spin fluctuations of a ferromagnetic reservoir. Our results show that collective relaxation rates of an ensemble of solid-state spin defects placed nearby a common ferromagnetic thin film can display clear signatures of superradiance and subradiance in the appropriate parameter regime. Furthermore, we find that the cooperative quantum behavior exhibits remarkable robustness against spatial disorder and thermal fluctuations. Our work lays the foundation for merging spintronics and quantum optics towards a common research horizon in the incoming future.

I. INTRODUCTION

Harnessing the unique properties of quantum mechanics has the potential to enable novel transformative technologies, such as quantum-enhanced sensors and scalable quantum networks that find applications ranging from cybersecurity to quantum analog simulations of complex solid-state systems [1–4]. Although significant progress has been achieved using superconducting qubits and trapped ions [5–8], the drawbacks of these front-runner technologies have generated a surge of interest in exploring alternative platforms. Solid-state spin defects, such as NV and Si-V centers in diamond, have attracted considerable attention as they display much longer coherence times than superconducting qubits and are optically active, which enables control via photonic channels and facilitates seamless integration with other photonic quantum technologies [9].

While solid-states spin defects can not couple to each other coherently at distances long enough to enable individual qubit manipulation [10–12], their interaction with nearby magnetic baths, which is routinely leveraged in quantum sensing schemes [13–19], has motivated several theoretical proposals for engineering quantum correlations between distant spin qubits via ancillary magnetic modes [20–23]. These earlier works focus on schemes to harbor coherent, i.e., energy-conserving, qubit-qubit coupling mediated by *virtual magnon processes*. To generate

sizable entanglement, however, the coherent qubit-qubit coupling has to be much larger than the local dissipation processes. Due to the strong relaxation effects induced by the interaction with the magnetic bath, developing scalable two-qubit gates using these quantum hybrid spin platforms remains a challenge.

While dissipative processes are detrimental in entanglement generation schemes relying on coherent interactions, recent progress at light-matter interfaces have shown that correlated dissipation can be harnessed to realize new dynamical states of matter and quantum applications [24–39]. In light-matter platforms, atomic emitters interact with each other through the emission or absorption of *real photons* in a shared photonic reservoir, as illustrated in Fig. 1. When multiple quantum emitters radiate in the shared bath, the collective spontaneous emission rate of an ensemble of atomic emitters may be enhanced (*superradiance*) or suppressed (*subradiance*) compared to that of an isolated emitter [40, 41], i.e., a signature of quantum cooperative behavior. The properties of superradiant and subradiant states are currently under intense investigation due to their potential for applications ranging from superradiant lasers [42, 43] to quantum-enhanced metrology [31, 44, 45] and quantum-information processing and storage [46, 47].

Inspired by these advancements, in this work we investigate the uncharted regime in which magnetic reservoirs can mediate dissipative correlations between solid-state spin defects via emission and absorption of *real magnons*, as shown in Fig. 1. While photons and magnons are bosonic excitations described by similar theoretical toolboxes, there are crucial differences in their physical prop-

* licqp@bc.edu

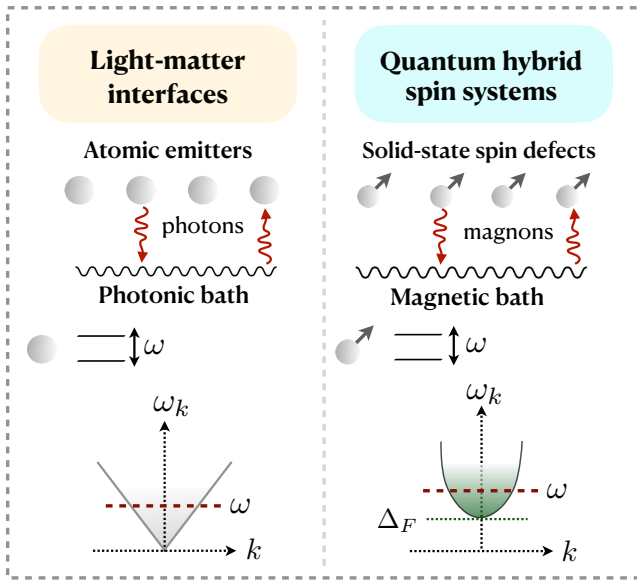


FIG. 1. Schematic illustration of the minimal ingredients to realizing cooperative quantum dynamics, i.e., an ensemble of long-lived quantum systems interacting via a shared reservoir. At light-matter interfaces, atomic emitters interact with each other via a shared photonic bath with dispersion ω_k . Since the resonance frequency ω of the quantum emitters is within the gapless photonic continuum, the quantum emitters can emit (absorb) *real photons* into (from) the bath. An analogous regime can be realized in quantum hybrid spin systems when the frequency ω of the solid-state spin defects is larger than the gap Δ_F of the spin-wave dispersion ω_k of the common magnetic reservoir. Previous proposals for entangling distant solid-state spin defects via magnetic modes focus on the opposite regime, i.e., $\omega < \Delta_F$ [20–23].

erties that can make them complementary in terms of experimental platforms. For example, the long wavelength of phonons makes them suitable for large systems, while magnons can provide a compact platform for on-chip nano-devices. Phonons are non-interacting, gapless, linearly dispersing bosonic excitations. Magnons, instead, are intrinsically interacting quasi-particles that display tunable band gaps and diverse dispersions owing to the rich plethora of magnetic materials. Furthermore, state-of-the-art spintronics techniques provide several pathways to engineering magnetic reservoirs, e.g., via spin current injection [48–51], thermal or electric biases [52]. It is thus natural to expect that harnessing quantum cooperativity in these solid-state hybrid quantum systems will unlock a novel set of functionalities and regimes. Importantly, probing correlated dissipative interactions in ensembles of quantum sensors interacting via a solid-state reservoir might enable to sense reservoir properties that are fundamentally unavailable to single-qubit sensors, potentially propelling a novel sensing modality forward.

In this work, we develop a comprehensive and versatile description of the many-body quantum dynamics of an

array of solid-state spin defects interacting via a shared magnetic bath. To understand whether correlated dissipation can play a relevant role in a realistic experimental setup, we apply our general framework to an ensemble of nitrogen vacancy (NV) centers coupled via a simple common magnetically ordered reservoir, i.e., a $U(1)$ -symmetric homogeneous ferromagnetic film at thermal equilibrium. Our findings suggest that clear experimental signatures of superradiant and subradiant behavior can be detected in the collective relaxation rate of the solid-state spin defect ensemble. We also explore the impact of finite temperatures and spatial distribution randomness and show that the cooperative phenomena remain remarkably robust in the face of these experimental perturbations.

On the one hand, our findings possess the potential to facilitate a profound knowledge transfer from the realm of cooperative quantum optics to the domain of quantum processing using solid-state devices. At the same time, our investigation reveals that, in conjunction with correlated emission, the NV ensemble is susceptible to correlated pumping processes and correlated dephasing. Both of these mechanisms pose challenges that are formidable, if not insurmountable, in terms of replication within atom-light matter interfaces. Consequently, this would set condensed matter systems as more adaptable platforms for dissipative many-body state preparation. A novel avenue arising from our work centers around the ability to dynamically control the bath that induces correlated dissipation — a control factor to a large extent absent in quantum optics. While the continuum of electromagnetic modes responsible for phenomena like super- and sub-radiance constitutes an inherent entity, magnetic materials and their magnonic excitations can be steered by currents, gradients in chemical potentials, and a range of other non-equilibrium driving knobs [53–55]. This naturally paves the way for studying cooperative phenomena and structured dissipation in the presence of far-from-equilibrium baths, which would not have counterparts in atomic arrays and could only be partially attainable in cavity quantum electrodynamics [56] or photonic waveguides [57]. We further elaborate on these directions in the concluding section of the manuscript.

This work is organized as follows. In Sec. II, we develop a general theoretical framework for the quantum many-body dynamics of an array of solid-state spin defects interacting via the magnetic field fluctuations of a shared solid-state reservoir. In Sec. III, we apply this formalism to a ferromagnetic bath and investigate the effective qubit-qubit interactions in experimentally relevant regimes. In Sec. IV, we explore the dynamics of the quantum hybrid spin system in the lowest Dicke, i.e., single-excitation, manifold. In Sec. V, we investigate the quantum many-body dynamics of the ensemble and its robustness to experimental perturbations, as well as the correlations of many-body states. We provide a summary

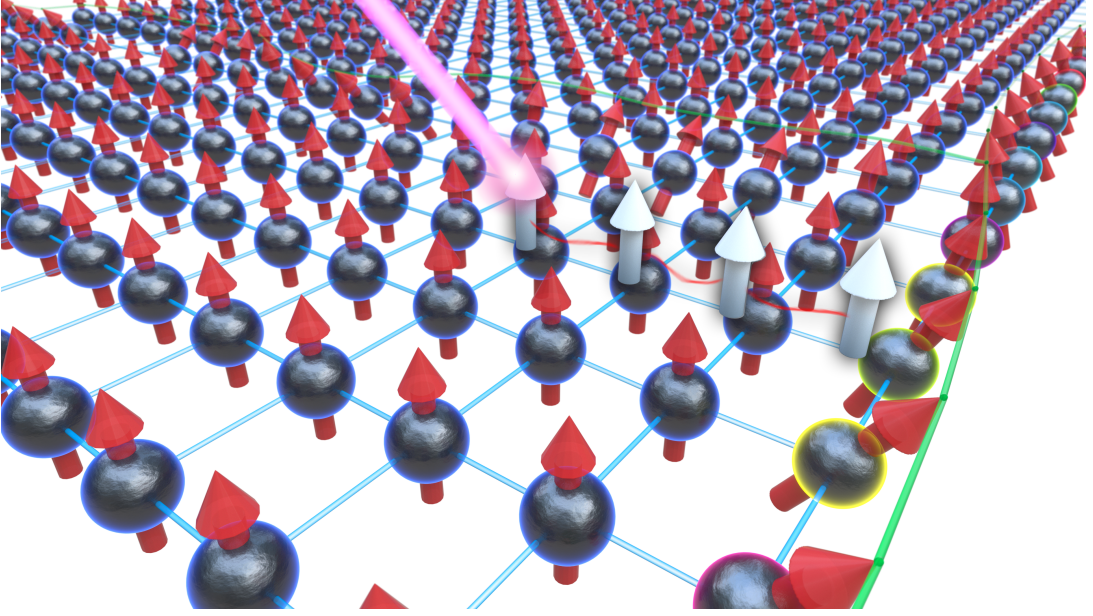


FIG. 2. Schematic setup for the qubit-qubit correlations mediated by the spin waves of a magnetic reservoir. The blue square lattice represents the magnet, with the red arrows indicating the ground state spin polarization and the green lines highlighting the spin-wave fluctuations. The spin qubits (grey arrows), which can be optically addressed, are arranged in a 1d array in a parallel plane above the magnetic lattice.

and outlook in Sec. VI.

II. MODEL

In this section, we address the quantum many-body dynamics of an array of solid-state spin defects interacting dissipatively via a solid-state reservoir. The starting point of our work is a one-dimensional (1d) array of solid-state spin defects, modeled as two-level systems, which couple to the magnetic field generated by a nearby reservoir. The Hamiltonian of the (isolated) qubit array reads as

$$\mathcal{H}_s = -\frac{1}{2} \sum_{\alpha} \omega_{\alpha} \boldsymbol{\sigma}_{\alpha} \cdot \hat{\mathbf{n}}_{\alpha}, \quad (1)$$

where $\hat{\mathbf{n}}_{\alpha} = (\sin \theta_{\alpha} \cos \phi_{\alpha}, \sin \theta_{\alpha} \sin \phi_{\alpha}, \cos \theta_{\alpha})$ labels the equilibrium orientation of the quantum spin $\boldsymbol{\sigma}_{\alpha}$ with resonance frequency ω_{α} residing the site \mathbf{r}_{α} . The Zeeman interaction between the qubit array and a magnetic field can be generally written as

$$\mathcal{H}_{SE} = -\tilde{\gamma} \sum_{\alpha} (B_{\alpha}^{+} \sigma_{\alpha}^{-} + B_{\alpha}^{-} \sigma_{\alpha}^{+} + B_{\alpha}^z \sigma_{\alpha}^z), \quad (2)$$

where $\tilde{\gamma}$ is the gyromagnetic ratio of the solid-state spin defects. The components $B_{\alpha}^{\pm} = B_{\alpha}^x \pm iB_{\alpha}^y$ and B_{α}^z correspond to the local stray field experienced by the α -th spin. Additionally, $\sigma_{\alpha}^{\pm} = (\sigma_{\alpha}^x \pm i\sigma_{\alpha}^y)/2$ and σ_{α}^z are the Pauli matrices expressed in the local coordinates of the α th qubit.

The interactions between a solid-state spin defect and the field fluctuations of a nearby solid-state reservoir are much weaker than the characteristic energy scales of the individual systems. Thus, the evolution of the density matrix ρ of the array can be generally described by the following Markovian master equation [58–64]

$$\frac{d\rho}{dt} = -i[\mathcal{H}_s + \mathcal{H}, \rho] + \mathcal{L}[\rho], \quad (3)$$

where the Hamiltonian \mathcal{H} reads as

$$\mathcal{H} = \sum_{\alpha, \beta} \sum_{(\mu, \tilde{\mu})} \sum_{(\nu, \tilde{\nu})} Y_{\alpha\beta}^{\mu\nu} \sigma_{\alpha}^{\tilde{\mu}} \sigma_{\beta}^{\tilde{\nu}}, \quad (4)$$

and

$$\mathcal{L}[\rho] = -\sum_{\alpha, \beta} \sum_{(\mu, \tilde{\mu})} \sum_{(\nu, \tilde{\nu})} X_{\alpha\beta}^{\mu\nu} (\{\rho, \sigma_{\alpha}^{\tilde{\mu}} \sigma_{\beta}^{\tilde{\nu}}\} - 2\sigma_{\beta}^{\tilde{\nu}} \rho \sigma_{\alpha}^{\tilde{\mu}}), \quad (5)$$

is the Lindbladian. Here, the sums over $(\mu, \tilde{\mu})$ and $(\nu, \tilde{\nu})$ are taken over the combinations $(\mu, \tilde{\mu}) = (\pm, \mp), (z, z)$, where $\pm = x \pm iy$. The explicit forms of $Y_{\alpha\beta}$ and $X_{\alpha\beta}$ are given by

$$Y_{\alpha\beta}^{\mu\nu} = \frac{\tilde{\gamma}^2}{2} \int_0^{\infty} d\tau G_{B_{\alpha}^{\mu} B_{\beta}^{\nu}}^{>}(\tau) e^{-i\omega_{\beta}^{\nu} \tau} - \frac{\tilde{\gamma}^2}{2} \int_0^{\infty} d\tau G_{B_{\beta}^{\nu} B_{\alpha}^{\mu}}^{<}(\tau) e^{-i\omega_{\alpha}^{\mu} \tau}, \quad (6)$$

$$X_{\alpha\beta}^{\mu\nu} = \frac{i\tilde{\gamma}^2}{2} \int_0^{\infty} d\tau G_{B_{\alpha}^{\mu} B_{\beta}^{\nu}}^{>}(\tau) e^{-i\omega_{\beta}^{\nu} \tau} + \frac{i\tilde{\gamma}^2}{2} \int_0^{\infty} d\tau G_{B_{\beta}^{\nu} B_{\alpha}^{\mu}}^{<}(\tau) e^{-i\omega_{\alpha}^{\mu} \tau}, \quad (7)$$

where the relevant frequencies are defined as $\omega_{\alpha(\beta)}^{\pm} = \pm\omega_{\alpha(\beta)}$ and $\omega_{\alpha(\beta)}^z = 0$, and the greater and lesser Green's functions follow the conventional definition [65] for two general operators \mathcal{O}_1 and \mathcal{O}_2 :

$$\begin{aligned} G_{\mathcal{O}_1, \mathcal{O}_2}^>(t) &\equiv -i\Theta(t)\langle\mathcal{O}_1(t)\mathcal{O}_2\rangle, \\ G_{\mathcal{O}_1, \mathcal{O}_2}^<(t) &\equiv -i\Theta(t)\langle\mathcal{O}_2\mathcal{O}_1(t)\rangle, \end{aligned} \quad (8)$$

where $\Theta(t)$ is the Heaviside step function.

The term $\propto Y_{\alpha\beta}$ (6) describes *coherent* qubit-qubit interactions that conserve the number of excitations, while the term $\propto X_{\alpha\beta}$ (7) represents the generator of the *incoherent dynamics*. Generally, incoherent processes have a *collective* character encoded in the off-diagonal elements of X (i.e., for $\alpha \neq \beta$), which are known to generate cooperative dynamics and entanglement at light-matter interfaces [30, 46, 66]. Furthermore, these terms encode nonlocal temporal and spatial correlations that conventional quantum sensing schemes, in which solid-state spin defects are operated as single-qubit sensing devices [67], can not access. For an isolated quantum spin, the second term on the right-hand side of Eq. (5) reduces to the *single-qubit* relaxation and dephasing rates routinely measured in quantum sensing experiments [14].

The formalism we have introduced here is rather general and can be applied to any solid-state reservoir whose fluctuating spin, pseudospin or charge degrees of freedom generate magnetic fields [68]. In this work, we focus on a qubit array interacting via long-range dipole-dipole interactions with a magnetically ordered bath, as shown in Fig. 2. Fluctuations of the spin density \mathbf{s}_r of the magnetic bath generate a stray field

$$\mathbf{B}_\alpha = \gamma \int d\mathbf{r} \mathcal{D}_{\mathbf{r}_\alpha, \mathbf{r}} \mathbf{s}_r, \quad (10)$$

where γ is the gyromagnetic ratio and $\mathcal{D}_{\mathbf{r}_\alpha, \mathbf{r}}$ is the tensorial Green's function of the magnetic dipolar field, which can be obtained as solutions of the Maxwell's equations in the magnetostatic limit [69]. Using Eq. (10) the greater (lesser) Green's functions in Eqs. (6) and (7) can be written as

$$G_{B_\alpha^\mu B_\beta^\nu}^{>(<)}(\tau) = \iint d^n\mathbf{r} d^n\mathbf{r}' \mathcal{D}_{\mathbf{r}, \mathbf{r}_\alpha}^{\mu\mu'} \mathcal{D}_{\mathbf{r}', \mathbf{r}_\beta}^{\nu\nu'} G_{\mathbf{s}_{\mathbf{r}}^{\mu'} \mathbf{s}_{\mathbf{r}'}^{\nu'}}^{>(<)}(\tau), \quad (11)$$

with $\mu, \nu = \pm, z$, and the repeated indices represent the Einstein summation. In the following, we discuss how symmetries that are relevant to common experimental realizations of the proposed setup allow to simplify the form of the master equation (3).

The magnetostatic Green's function $\mathcal{D}_{\mathbf{r}, \mathbf{r}_\alpha}^{\mu\nu}$ (10) represents the response of the magnetic bath at position \mathbf{r}_α to an external perturbation at position \mathbf{r} . For a bath with translational symmetry, the magnetostatic Green's function only depends on the relative position vector $\mathbf{r} - \mathbf{r}_\alpha$, i.e., $\mathcal{D}_{\mathbf{r}, \mathbf{r}_\alpha}^{\mu\nu} = \mathcal{D}_{\mathbf{r}-\mathbf{r}_\alpha}^{\mu\nu}$. Analogously, we can set $G_{\mathbf{s}_{\mathbf{r}}^{\mu'} \mathbf{s}_{\mathbf{r}'}^{\nu'}}^{>(<)}(\tau) = G_{\mathbf{s}_{\mathbf{r}}^{\mu'} \mathbf{s}_{\mathbf{r}-\mathbf{r}'}^{\nu'}}^{>(<)}(\tau, \mathbf{r} - \mathbf{r}')$. We can substitute the

Fourier transform of the magnetostatic Green's function, i.e.,

$$\mathcal{D}_{\mathbf{r}-\mathbf{r}_\alpha}^{\mu\nu} = \int \frac{d^n\mathbf{k}}{(2\pi)^n} \tilde{\mathcal{D}}_{\mathbf{k}}^{\mu\nu} e^{i\mathbf{k}\cdot(\mathbf{r}-\mathbf{r}_\alpha)}, \quad (12)$$

into Eq. (11), which leads to

$$G_{B_\alpha^\mu B_\beta^\nu}^{>(<)}(\tau) = \int \frac{d^n\mathbf{k}}{(2\pi)^n} e^{-i\mathbf{k}\cdot\boldsymbol{\rho}_{\alpha\beta}} \mathcal{G}^{\mu\nu}(\tau, \mathbf{k}), \quad (13)$$

where $\boldsymbol{\rho}_{\alpha\beta} = \mathbf{r}_\alpha - \mathbf{r}_\beta$ is the distance between the quantum spins $\boldsymbol{\sigma}_\alpha$ and $\boldsymbol{\sigma}_\beta$ and with

$$\mathcal{G}^{\mu\nu}(\tau, \mathbf{k}) = \tilde{\mathcal{D}}_{\mathbf{k}}^{\mu\mu'} \tilde{\mathcal{D}}_{-\mathbf{k}}^{\nu\nu'} \tilde{G}_{\mathbf{s}_{\mathbf{r}}^{\mu'} \mathbf{s}_{-\mathbf{r}}^{\nu'}}^{>(<)}(\tau, -\mathbf{k}), \quad (14)$$

where \mathbf{k} is the wavevector in Fourier space and $\tilde{\mathcal{D}}_{\mathbf{k}}$ and $\tilde{G}_{\mathbf{s}_{\mathbf{r}}^{\mu'} \mathbf{s}_{-\mathbf{r}}^{\nu'}}^{>(<)}(\mathbf{k})$ represent the Fourier-transformed Green's functions. Moreover, isotropy in the real space allows to further simplify $G_{\mathbf{s}_{\mathbf{r}}^{\mu'} \mathbf{s}_{-\mathbf{r}}^{\nu'}}^{>(<)}(\tau, \mathbf{r} - \mathbf{r}') = G_{\mathbf{s}_{\mathbf{r}}^{\mu'} \mathbf{s}_{-\mathbf{r}}^{\nu'}}^{>(<)}(\tau, |\mathbf{r} - \mathbf{r}'|)$.

Another symmetry relevant to several magnetic reservoirs is $U(1)$ symmetry, i.e., the symmetry under spin rotations around the direction of magnetic field (here taken to be along \mathbf{z}), which implies the conservation of the spin projection on the direction of magnetic field, i.e., the magnon number. While the magnon number is not a conserved quantity due to the ubiquitous spin nonconserving interactions of magnons with the crystalline lattice, it is generally taken to be *approximately* conserved in collinear magnetic systems that display low damping and strong number-conserving interactions [70]. This assumption allows to simplify our model further as the transverse spin response is completely decoupled from the longitudinal spin dynamics, i.e., $\langle \hat{s}^\pm(\mathbf{r}', t) \hat{s}^z(\mathbf{r}, 0) \rangle = 0$ and $\langle \hat{s}^\pm(\mathbf{r}', t) \hat{s}^\pm(\mathbf{r}, 0) \rangle = 0$. When the (equilibrium) spin density of the magnetic bath and the quantum spins are collinear, i.e., $\theta_\alpha = 0$ for $\alpha = 1, \dots, N$, the whole system is $U(1)$ -symmetric, and only two-point correlations of the form $\langle B^- B^+ \rangle$, $\langle B^+ B^- \rangle$, and $\langle B^z B^z \rangle$ are not vanishing.

As a consequence of these symmetries, the Hamiltonian (4) takes the form of an XXZ model with long-range couplings, i.e.,

$$\mathcal{H} = \sum_{\alpha \neq \beta} J_{\alpha\beta} \sigma_\alpha^+ \sigma_\beta^- + \sum_{\alpha \neq \beta} J_{\alpha\beta}^z \sigma_\alpha^z \sigma_\beta^z, \quad (15)$$

with

$$J_{\alpha\beta} = \frac{\tilde{\gamma}^2}{2} \left[G_{B_\alpha^- B_\beta^+}^R(-\omega_\beta) + G_{B_\beta^+ B_\alpha^-}^R(\omega_\alpha) \right], \quad (16)$$

$$J_{\alpha\beta}^z = \frac{\tilde{\gamma}^2}{4} \left[G_{B_\alpha^- B_\beta^+}^R(0) + G_{B_\beta^+ B_\alpha^-}^R(0) \right], \quad (17)$$

where we have neglected the overall energy shift proportional to $\mathcal{H}_{\text{const}} = \sum_\alpha (J_{\alpha\alpha}^- + J_{\alpha\alpha}^+ + 2J_{\alpha\alpha}^{zz}) \sigma_\alpha^0/2$ and the Lamb shift proportional to $\sum_\alpha J_L^\alpha \sigma_\alpha^z$. Here the retarded Green's function for two general operators \mathcal{O}_1 and \mathcal{O}_2 is defined as

$$G_{\mathcal{O}_1\mathcal{O}_2}^R(\tau) = -i\Theta(\tau)\langle[\mathcal{O}_1(\tau), \mathcal{O}_2]\rangle, \quad (18)$$

where $\Theta(\tau)$ is the Heaviside step function and $[\mathcal{O}_1(\tau), \mathcal{O}_2] = \mathcal{O}_1(\tau)\mathcal{O}_2 - \mathcal{O}_2\mathcal{O}_1(\tau)$. The Lindbladian operator (5) simplifies to

$$\begin{aligned} \mathcal{L}[\rho] = & \sum_{\alpha\beta} \left[\Gamma_{\alpha\beta} \left(\{\sigma_{\alpha}^{-}\sigma_{\beta}^{+}, \rho\} - 2\sigma_{\beta}^{+}\rho\sigma_{\alpha}^{-} \right) \right. \\ & + \tilde{\Gamma}_{\alpha\beta} \left(\{\sigma_{\alpha}^{+}\sigma_{\beta}^{-}, \rho\} - 2\sigma_{\beta}^{-}\rho\sigma_{\alpha}^{+} \right) \\ & \left. + \Gamma_{\alpha\beta}^z \left(\{\sigma_{\alpha}^z\sigma_{\beta}^z, \rho\} - 2\sigma_{\beta}^z\rho\sigma_{\alpha}^z \right) \right], \quad (19) \end{aligned}$$

where the curly brackets $\{\mathcal{O}_{\alpha}, \mathcal{O}_{\beta}\}$ represents the anti-commutator $\{\mathcal{O}_{\alpha}, \mathcal{O}_{\beta}\} = \mathcal{O}_{\alpha}\mathcal{O}_{\beta} + \mathcal{O}_{\beta}\mathcal{O}_{\alpha}$ and, for notational convenience, we have redefined $\Gamma_{\alpha\beta} = X_{\alpha\beta}^{+-}$, $\tilde{\Gamma}_{\alpha\beta} = X_{\alpha\beta}^{-+}$ and $\Gamma_{\alpha\beta}^z = X_{\alpha\beta}^{zz}$.

For an ensemble of qubits with identical transition frequencies, denoted as $\omega_{qi} = \omega_{\alpha}$ for $\alpha = 1, \dots, N$, the coefficients in the Lindbladian (19) can be further simplified to

$$\Gamma_{\alpha\beta} = i\frac{\tilde{\gamma}^2}{2}G_{B_{\alpha}^{+}B_{\beta}^{-}}^{>}(\omega_{qi}), \quad (20)$$

$$\tilde{\Gamma}_{\alpha\beta} = i\frac{\tilde{\gamma}^2}{2}G_{B_{\beta}^{+}B_{\alpha}^{-}}^{<}(\omega_{qi}), \quad (21)$$

$$\Gamma_{\alpha\beta}^z = i\frac{\tilde{\gamma}^2}{2}G_{B_{\alpha}^zB_{\beta}^z}^{>}(0). \quad (22)$$

For an individual qubit, i.e., $\alpha = \beta$, the coefficients $\Gamma_{\alpha\alpha} \equiv \Gamma_0$ and $\tilde{\Gamma}_{\alpha\alpha} \equiv \tilde{\Gamma}_0$ govern the local relaxation rate, while $\Gamma_{\alpha\alpha}^z \equiv \Gamma_0^z$ reduces to the local dephasing rate. At thermal equilibrium, the fluctuation-dissipation theorem relates Eqs. (20) and (21) as $\tilde{\Gamma}_{\alpha\beta} = e^{-\beta\hbar\omega_{qi}}\Gamma_{\alpha\beta}$, where $\beta = 1/(k_B T)$, k_B is the Boltzmann constant, T is the temperature, and \hbar is the reduced Planck's constant [71]. The term $\propto \tilde{\Gamma}_{\alpha\beta}$ describes the spin-qubit absorption of spin angular momentum from the thermal reservoir: at zero temperature, this term vanishes since there are no thermally populated magnons in the film. Only the reverse process $\propto \Gamma_{\alpha\beta}$, i.e., the emission of magnons from the qubits into the magnetic bath, can occur.

Invoking the fluctuation-dissipation theorem allows to rewrite Eqs. (20) and (22) as

$$\Gamma_{\alpha\beta} = \gamma^2\tilde{\gamma}^2[n_B(\omega_{qi}) + 1] \int \frac{d^n\mathbf{k}}{(2\pi)^n} e^{-i\mathbf{k}\cdot\boldsymbol{\rho}_{\alpha\beta}} \tilde{\Gamma}(\omega_{qi}, \mathbf{k}), \quad (23)$$

$$\Gamma_{\alpha\beta}^z = \gamma^2\tilde{\gamma}^2[n_B(0) + 1] \int \frac{d^n\mathbf{k}}{(2\pi)^n} e^{-i\mathbf{k}\cdot\boldsymbol{\rho}_{\alpha\beta}} \tilde{\Gamma}(0, \mathbf{k}), \quad (24)$$

where

$$\begin{aligned} \tilde{\Gamma}(\omega_{qi}, \mathbf{k}) = & \tilde{\mathcal{D}}_{\mathbf{k}}^{-+}\tilde{\mathcal{D}}_{-\mathbf{k}}^{+-}\text{Im}[\chi^{+-}(\omega_{qi}, \mathbf{k})] \\ & + \tilde{\mathcal{D}}_{\mathbf{k}}^{-+}\tilde{\mathcal{D}}_{-\mathbf{k}}^{+-}\text{Im}[\chi^{-+}(\omega_{qi}, \mathbf{k})] \\ & + \tilde{\mathcal{D}}_{\mathbf{k}}^{-z}\tilde{\mathcal{D}}_{-\mathbf{k}}^{+z}\text{Im}[\chi^{zz}(\omega_{qi}, \mathbf{k})]. \quad (25) \end{aligned}$$

Here, $\text{Im}[\chi^{\mu\nu}(\omega_{qi}, \mathbf{k})]$ denotes the real part of the dynamical spin susceptibility tensor χ , which is defined as

$$\chi^{\mu\nu}(\omega_{qi}, \mathbf{k}) = \tilde{G}_{s^{\mu}s^{\nu}}^R(\omega_{qi}, \mathbf{k}), \quad (26)$$

where $\tilde{G}_{s^{\mu}s^{\nu}}^R(\omega_{qi}, \mathbf{k})$ is the retarded Green's function in momentum space. Similarly, we can rewrite the coherent couplings (16) and (17) as

$$J_{\alpha\beta} = \frac{\gamma^2\tilde{\gamma}^2}{2} \int \frac{d^n\mathbf{k}}{(2\pi)^n} e^{-i\mathbf{k}\cdot\boldsymbol{\rho}_{\alpha\beta}} \tilde{J}(\omega_{qi}, \mathbf{k}), \quad (27)$$

$$J_{\alpha\beta}^z = \frac{\gamma^2\tilde{\gamma}^2}{4} \int \frac{d^n\mathbf{k}}{(2\pi)^n} e^{-i\mathbf{k}\cdot\boldsymbol{\rho}_{\alpha\beta}} \tilde{J}(0, \mathbf{k}), \quad (28)$$

with

$$\begin{aligned} \tilde{J}(\omega_{qi}, \mathbf{k}) = & \tilde{\mathcal{D}}_{\mathbf{k}}^{-+}\tilde{\mathcal{D}}_{-\mathbf{k}}^{+-}\text{Re}[\chi^{+-}(\omega_{qi}, \mathbf{k})] \\ & + \tilde{\mathcal{D}}_{\mathbf{k}}^{-+}\tilde{\mathcal{D}}_{-\mathbf{k}}^{+-}\text{Re}[\chi^{-+}(\omega_{qi}, \mathbf{k})] \\ & + \tilde{\mathcal{D}}_{\mathbf{k}}^{-z}\tilde{\mathcal{D}}_{-\mathbf{k}}^{+z}\text{Re}[\chi^{zz}(\omega_{qi}, \mathbf{k})]. \quad (29) \end{aligned}$$

III. FERROMAGNETIC BATH

We will now apply the framework developed in the previous section to explore the properties of a qubit array interacting via a simple common magnetic reservoir, i.e., a $U(1)$ -symmetric homogeneous ferromagnetic film. The key quantity controlling the effective qubit-qubit coupling is the dynamical spin susceptibility χ of the magnetic bath, which describes its linear response to an externally applied time-dependent perturbation \mathbf{h} . The susceptibility χ is a tensor that in general couples all components of the spin response to each other. For a $U(1)$ -symmetric system, however, the full response decouples into a longitudinal and transverse part. The transverse response can be compactly described using the circular combinations $s^{\pm} = (s^x \pm is^y)/2$ and $h^{\pm} = h^x \pm ih^y$, yielding for the $-$ component

$$s^{-}(\omega, k) = \chi^{-+}(\omega, k)h^{-}(\omega, k), \quad (30)$$

with $\chi^{+-}(\omega, k) = [\chi^{-+}(-\omega, k)]^*$. Similarly, the longitudinal spin susceptibility $\chi^{zz}(\omega, k)$ can be introduced as

$$s^z(\omega, k) = \chi^{zz}(\omega, k)h^z(\omega, k). \quad (31)$$

Recalling Eq. (26) and introducing the Holstein-Primakoff transformation, i.e., $s^{-} = s - a^{\dagger}a$ and $s^{+} \simeq \sqrt{2s}a^{\dagger}$, the transverse (30) and longitudinal (31) spin susceptibilities can be straightforwardly related to, respectively, two-point and four-point magnon correlation functions. The transverse spin susceptibility (30) is proportional to the magnon density of states. Thus, its contribution to the dissipative qubit-qubit couplings (25) is associated with the emission (absorption) of a single magnon with energy equal to the qubit frequency ω_{qi}

into (from) the bath. The longitudinal spin susceptibility (31), instead, encodes two-magnon (Raman) processes, i.e., a magnon scattering with energy gain (or loss) equal to the frequency ω_{qi} of the solid-state spin defect [16].

In the long-wavelength limit, the dynamical transverse magnetic response can be extracted from the Landau–Lifshitz–Gilbert (LLG) equation [72]:

$$\frac{d\mathbf{s}}{dt} = -\gamma\mathbf{s} \times \mathbf{B}_{eff} + \frac{\alpha}{s}\mathbf{s} \times \frac{d\mathbf{s}}{dt} - \gamma\mathbf{s} \times \mathbf{h}, \quad (32)$$

where α is the dimensionless Gilbert damping parameter and $\mathbf{B}_{eff} = -\gamma^{-1}\partial\mathcal{H}[\mathbf{s}]/\partial\mathbf{s}$ is the effective magnetic field containing the contributions from an external magnetic field $\mathbf{B}_0 = B_0\hat{\mathbf{z}}$ as well as internal magnetic fields originating from the interaction of the spin density with its surrounding. Here we consider a 2d ferromagnetic reservoir with Heisenberg exchange interaction J and uniaxial anisotropy A , described by the following Hamiltonian

$$\mathcal{H}[\mathbf{s}] = \int d^2\mathbf{r} \left[-J\mathbf{s}(\mathbf{r}) \cdot \nabla^2\mathbf{s}(\mathbf{r}) - A(\mathbf{s}(\mathbf{r}) \cdot \hat{\mathbf{z}})^2 - \gamma B_0\mathbf{s}(\mathbf{r}) \cdot \hat{\mathbf{z}} \right]. \quad (33)$$

The energy spectrum of the spin waves obeying Eq. (33) reads as

$$\omega_F(k) = Dk^2 + \Delta_F, \quad (34)$$

where $D = \gamma s J$ represents the spin stiffness and $\Delta_F = 2\gamma A s + \gamma B_0$ is the spin-wave gap. In the following, we focus on the regime in which one-magnon processes can take place by setting the qubit frequency to be larger than the spin-wave gap, i.e., $\omega_{qi} > \Delta_F$.

We assume that the magnetic field is large enough to align the spin density along its direction, i.e., $\mathbf{s} = (s_x, s_y, s)$, with $|\mathbf{s}| \simeq s$, and proceed to linearize Eq. (32) around the equilibrium direction of the magnetic order parameter. Upon Fourier transform, we can recast Eq. (32) in the form of Eq. (30), which allows us to identify

$$\chi^{-+}(\omega, k) = \frac{s}{D(k^2 - 1/\lambda^2) - i\alpha\omega}, \quad (35)$$

where λ is a characteristic magnon wavelength defined as $\lambda = \sqrt{D/(\omega - \Delta_F)}$.

Invoking the relation $\chi^{+-}(\omega, k) = [\chi^{-+}(-\omega, k)]^*$, we find

$$\chi^{+-}(\omega, k) = \frac{s}{D(k^2 + 1/\lambda'^2) - i\alpha\omega}, \quad (36)$$

with $\lambda' = \sqrt{D/(\omega + \Delta_F)}$. The longitudinal spin susceptibility of the magnetic bath can not be captured by the LLG formalism (32), but depends instead on the pertinent spin transport regime [16, 73, 74]. At wavelengths larger than the magnon mean free path, the dynamics of

the longitudinal spin density s_z can be treated as diffusive [53], i.e.,

$$\frac{ds_z}{dt} + \nabla \cdot \mathbf{j}_s = -\frac{s_z}{\tau_s}, \quad (37)$$

Here, we have introduced the spin-relaxation time τ_s and the spin current $\mathbf{j}_s = -\sigma\nabla\mu$, where σ is the magnon spin conductivity, $\mu = \chi_0^{-1}s_z - \gamma h^z$ the chemical potential, and χ_0 the static uniform longitudinal susceptibility. Recasting Eq. (37) in terms of Eq. (31), one can identify

$$\chi^{zz}(\omega, k) = \frac{\chi_0(l_s^{-2} + k^2)}{-i\omega(\chi_0/\sigma) + (l_s^{-2} + k^2)}, \quad (38)$$

where $l_s = \sqrt{\sigma\tau_s/\chi_0}$ is the spin diffusion length. In the regime of interest, i.e., $\omega_{qi} > \Delta_F$, the process dominating the relaxation dynamics of the spin defects is the emission (absorption) of a real magnon with frequency ω_{qi} in (from) the magnetic bath [16]. Thus, in what follows, we focus on the contributions to the dissipative couplings (25) stemming from the transverse susceptibilities (35) and (36), and neglect the two-magnon processes described by Eq. (38). It is worth noting, however, that several magnetic systems, e.g., most antiferromagnets, display a spin-wave gap Δ_F far larger than the typical solid-state spin-defect resonance frequency ω_{qi} . Whether two-magnon scattering processes can mediate quantum cooperative behavior in these systems is an intriguing question that we will address in future investigations.

IV. MASTER EQUATION

We proceed to derive the master equation describing the dynamics of the density matrix of the qubit array interacting via a simple ferromagnetic reservoir. We focus on the regime in which the energy exchange between the ferromagnetic film and the qubit array is dominated by single-magnon processes, i.e., $\omega_{qi} > \Delta_F$, and neglect the two-magnon (Raman) scattering processes described by Eq. (38). For concreteness, we consider a Yttrium Iron Garnet (YIG) film of thickness $L = 10$ nm, spin stiffness $D = 4.3 \times 10^{-30}$ erg·cm², Gilbert damping parameter $\alpha \approx 1 \times 10^{-4}$, saturation surface spin density $s = 8 \times 10^{-12}$ G²·cm·s and spin-wave gap $\Delta_F = K + \gamma B_0$, with zero-field gap $K = 3.296 \times 10^{-18}$ erg. As solid-state spin-defects, we consider an ensemble of NV centers. While the latter form a spin-triplet system in the ground state, by applying an external magnetic field $B_0\hat{\mathbf{z}}$ along their principal axis, here taken to be the $\hat{\mathbf{z}}$ axis, the degeneracy between $m_s = \pm 1$ can be lifted and we can approximate each qubit as a two-level system with frequency $\omega_{qi} = \Delta_0 - \gamma B_0$, where $\Delta_0 = 2.87$ GHz = 1.9×10^{-17} erg is the NV-center zero-field splitting. Such an approximation is valid as long as the thermal energy of the system is far smaller than the energy of the higher NV-center transition, i.e.,

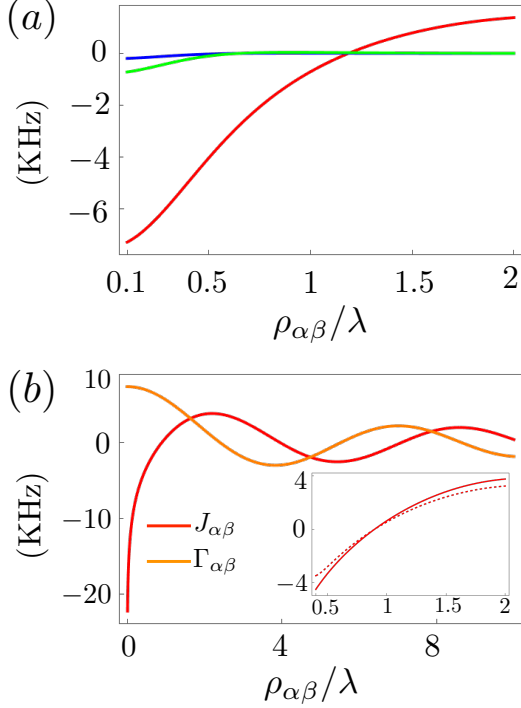


FIG. 3. (a) The green, red and blue curves display the dependence of, respectively, the coherent Ising coupling (41), the first and second terms on the right hand-side of Eq. (40) on the interqubit separation $\rho_{\alpha\beta}$ (in units of the wavelength λ). (b) The red and yellow curves show the dependence of, respectively, the coherent $J_{\alpha\beta}$ (43) and incoherent $\Gamma_{\alpha\beta}$ (42) couplings on the interqubit separation $\rho_{\alpha\beta}$. Inset: comparison between Eq. (40) (red dashed curve) and the approximation provided by Eq. (43) (red solid curve). In each figure, the parameters used are for an ensemble of NV-center spins interacting via a YIG thin film at $T = 0$.

$k_B T \ll \Delta_0 + \gamma B_0$, which is consistent with the quantum regime we are focusing on.

We set the distance between the YIG film and the NV-center ensemble to be $d = 30$ nm: interactions between the spin-wave fluctuations of YIG and NV-center spin defects have been already successfully leveraged in several quantum sensing experiments at even larger distances [17, 19]. The full master equation can be derived by plugging Eqs. (35) and (36) into Eqs. (25) and (29). In the limit of weak Gilbert damping, i.e., $\alpha \ll 1$, the master equation (3) reduces to

$$\begin{aligned} \frac{d\rho}{dt} = & -i \sum_{\alpha \neq \beta} \left[J_{\alpha\beta} \sigma_{\alpha}^{+} \sigma_{\beta}^{-} + J_{\alpha\beta}^z \sigma_{\alpha}^z \sigma_{\beta}^z, \rho \right] \\ & + \sum_{\alpha\beta} \Gamma_{\alpha\beta} \left(\{ \sigma_{\alpha}^{-} \sigma_{\beta}^{+}, \rho \} - 2 \sigma_{\beta}^{+} \rho \sigma_{\alpha}^{-} \right) \\ & + \sum_{\alpha\beta} \tilde{\Gamma}_{\alpha\beta} \left(\{ \sigma_{\alpha}^{+} \sigma_{\beta}^{-}, \rho \} - 2 \sigma_{\beta}^{-} \rho \sigma_{\alpha}^{+} \right), \quad (39) \end{aligned}$$

with

$$J_{\alpha\beta}/\nu = -\frac{1}{2} \left[\frac{\omega_{qi} - \Delta_F}{\Delta_0} P.V. \int_0^{\infty} d\xi \xi^3 \frac{J_0(\xi \frac{\rho_{\alpha\beta}}{\lambda}) e^{-\frac{2d}{\lambda'} \xi}}{\xi^2 - 1} + \frac{\omega_{qi} + \Delta_F}{\Delta_0} \int_0^{\infty} d\xi \xi^3 \frac{J_0(\xi \frac{\rho_{\alpha\beta}}{\lambda'}) e^{-\frac{2d}{\lambda'} \xi}}{\xi^2 + 1} \right], \quad (40)$$

$$J_{\alpha\beta}^z/\nu = -\frac{\Delta_F}{\Delta_0} \int_0^{\infty} d\xi \xi^3 \frac{e^{-\frac{2d}{\lambda_{exc}} \xi} J_0(\xi \frac{\rho_{\alpha\beta}}{\lambda_{exc}})}{\xi^2 + 1}, \quad (41)$$

$$\Gamma_{\alpha\beta}/\nu = \frac{\pi [n_B(\omega_{qi}) + 1]}{4} \frac{\omega_{qi} - \Delta_F}{\Delta_0} J_0\left(\frac{\rho_{\alpha\beta}}{\lambda}\right) e^{-\frac{2d}{\lambda}}. \quad (42)$$

Here we have introduced $\lambda_{exc} = \sqrt{D/\Delta_F}$, and $\nu = \frac{\pi \hbar^2 (\gamma \tilde{\gamma})^2 s \Delta_0}{D^2}$ is a characteristic frequency controlling the strength of coherent and dissipative interactions. The dissipative channels in Eq. (39) contain both correlated emission and correlated pump channels: the probability that a NV emits (absorbs) a magnon influences the occurrence of an analog event for another NV at a distance set by the spatial structure of the Γ ($\tilde{\Gamma}$) factors in (39). This is at variance with quantum optics platforms where only the former can naturally occur [25] or be engineered with Raman sidebands [75]. The occurrence of a novel form of correlated dissipation is one of the extra leverages offered by solid-state platforms, showing that the cooperative mechanisms expounded in this study transcend a mere one-to-one correspondence with quantum optics.

An ultimate goal would be to realize a quantum hybrid platform in which cooperative quantum dynamics survives at interqubit distances that allow for individual qubit addressability. Equation (42) shows that the strength of dissipative interactions is controlled by the characteristic wavelength $\lambda = \sqrt{D/(\omega_{qi} - \Delta_F)}$, which can be maximized by choosing a material with large spin stiffness D , i.e., high Curie temperature T_c . However, it is important to note that the strength of interactions scales $\nu \propto D^{-2}$, i.e., the spin-wave fluctuations to which qubits can couple become weaker in stiffer materials. Alternatively, one can minimize the detuning between the NV-center resonance frequency ω_{qi} and the spin-wave gap Δ_F via an external magnetic field B_0 , i.e., $\omega_{qi} - \Delta_F = \Delta_0 + K - 2\gamma B_0$. By choosing $B \sim 40$ mT, we set $\omega_{qi} - \Delta_F \sim 10$ MHz, consistently with the experimental frequency resolution limits. In this regime, we find $\lambda \sim 80$ nm and $\lambda', \lambda_{exc} \sim 5$ nm.

From Fig. 3(a) it is clear that spatial decay of the coherent Ising coupling (41) (green curve), which is controlled by the wavelength λ_{exc} , is very rapid compared to the first term on the right-side of Eq. (40) (red curve). Therefore, we set $J_z = 0$ as it does not play a substantial role in the quantum dynamics we are interested in. Figure 3(a) shows also that the strength of the first term on the right-side of Eq. (40) (red curve), whose decay is controlled by the wavelength λ , is much larger than the second term on the right-hand side of Eq. (40) (blue curve), which scales with the wavelength λ' . We therefore retain only the first term on the right-side of Eq. (40) and

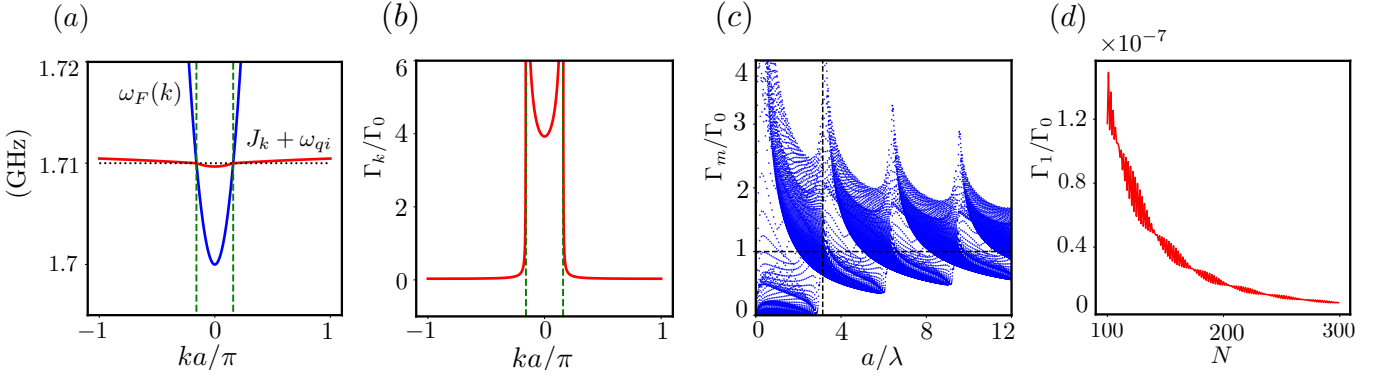


FIG. 4. (a) Dispersion relation $J_k + \omega_{qi}$ for the single-excitation modes of an infinite, one-dimensional chain (red line). The blue line represents the spin-wave dispersion $\omega_F(k)$ of the magnetic film (34), while the black dashed line corresponds to the resonance frequency ω_{qi} of the qubits. (b) Collective decay rate Γ_k of the qubit array normalized by the relaxation rate Γ_0 of a noninteracting array. The green dashed lines separate subradiant from superradiant modes. (c) Normalized decay rates Γ_m at different lattice constants a/λ for a finite array of $N = 40$ solid-state spin defects. Subradiant modes with relaxation rates approaching zero arise only for $a/\lambda < \pi$ (vertical dashed line), in agreement with the infinite chain analysis. (d) The decay rate of the most subradiant eigenmode as function of the number of qubits for $a/\lambda = 0.1$. In each figure, the parameters used are for an ensemble of NV-center spins interacting via a YIG thin film.

take the limit $e^{-\frac{2d}{\lambda}} \rightarrow 1$, which allows to rewrite Eq. (40) as

$$J_{\alpha\beta}/\nu = \frac{\pi}{4} \frac{\omega_{qi} - \Delta_F}{\Delta_0} Y_0 \left(\frac{\rho_{\alpha\beta}}{\lambda} \right). \quad (43)$$

As shown by the inset of Fig. 3(b), Eq. (43) (solid red curve) is a good approximation of Eq. (40) (dashed red curve) within the selected parameter regime. Therefore, Eq. (39) can be rewritten as

$$\begin{aligned} \frac{d\rho}{dt} = & -i \sum_{\alpha \neq \beta} \left[J_{\alpha\beta} \sigma_{\alpha}^{+} \sigma_{\beta}^{-}, \rho \right] \\ & + \sum_{\alpha\beta} \Gamma_{\alpha\beta} \left(\{ \sigma_{\alpha}^{-} \sigma_{\beta}^{+}, \rho \} - 2 \sigma_{\beta}^{+} \rho \sigma_{\alpha}^{-} \right) \\ & + \sum_{\alpha\beta} \tilde{\Gamma}_{\alpha\beta} \left(\{ \sigma_{\alpha}^{+} \sigma_{\beta}^{-}, \rho \} - 2 \sigma_{\beta}^{-} \rho \sigma_{\alpha}^{+} \right). \end{aligned} \quad (44)$$

where the strength of dissipative and coherent interactions is given, respectively, by Eqs. (40) and (43), while thermal equilibrium requires $\tilde{\Gamma}_{\alpha\beta} = e^{-\beta \hbar \omega_{qi}} \Gamma_{\alpha\beta}$.

Figure 3(b) shows that when the qubits are very close to each other, i.e., $\rho_{\alpha\beta} \rightarrow 0$, the coherent exchange interaction $J_{\alpha\beta}$ (red curve) becomes significantly larger compared to the dissipative coupling $\Gamma_{\alpha\beta}$ (orange curve). However, as we are interested in maximizing the interqubit separation, here we focus on the regime in which the interqubit distance $\rho_{\alpha\beta}$ approaches the characteristic wavelength, i.e., $\rho_{\alpha\beta} \sim \lambda$. In this regime, the exchange interaction $J_{\alpha\beta}$ becomes comparable to the decoherence rate $\Gamma_{\alpha\beta}$, i.e., $J_{\alpha\beta} \sim \Gamma_{\alpha\beta}$, suggesting that dissipative correlations might play a relevant role in the quantum many-body dynamics of the qubit array.

V. SINGLE-EXCITATION SECTOR

In order to gain analytical insights into our model, we analyze the single-excitation sector, corresponding to the qubit array sharing a single spin excitation. For vanishing temperature, i.e., $T \rightarrow 0$, Eq. (44) can be written as

$$\frac{d\rho}{dt} = -i[\mathcal{H}_{eff}, \rho] + \sum_{\alpha\beta} 2\Gamma_{\alpha\beta} \sigma_{\beta}^{+} \rho \sigma_{\alpha}^{-}, \quad (45)$$

where we have introduced the effective non-Hermitian Hamiltonian defined as $\mathcal{H}_{eff} = \mathcal{H} + \mathcal{H}_{nh}$ with $\mathcal{H}_{nh} = -i \sum_{\alpha\beta} \Gamma_{\alpha\beta} \sigma_{\alpha}^{-} \sigma_{\beta}^{+}$. The impact of finite temperature will be discussed in Sec. VIB. In the single-excitation sector, one can neglect the quantum jump terms, i.e., the second term on the right-hand side of Eq. (45) [61]. Thus, when a single qubit is initialized in the excited state, the density matrix dynamics is well-described by an effective non-Hermitian Hamiltonian \mathcal{H}_{eff} , which suggests that the proposed quantum hybrid spin systems might also provide a novel testbed for exploring non-Hermitian magnonic phenomena [76–84] as well as their robustness against many-body quantum effects [85].

In our analysis, we first consider an infinite chain of solid-state spin defects: even though this scenario is not realistic, it will allow us to gain key insights into the physical properties of the system. In the limit $N \rightarrow \infty$, the eigenstates of the effective non-Hermitian Hamiltonian \mathcal{H}_{eff} are spin waves characterized by a well-defined quasimomentum k . The single-excitation eigenstates, which are delocalized and shared coherently by all the qubits, can be written as $\sigma_{\alpha}^{+} = (1/\sqrt{N}) \sum_k e^{ikr_{\alpha}} S_k$, where S_k is the spin-wave annihilation operator.

In this quasimomentum representation, the effective

Hamiltonian takes the form:

$$\mathcal{H}_{eff}(k) = \sum_k (J_k - i\Gamma_k) S_k^\dagger S_k, \quad (46)$$

where the coefficients J_k and Γ_k are defined as

$$J_k = \sum_{n=\pm 1}^{\pm\infty} J(|n|a) e^{-in ka}, \quad (47)$$

$$\Gamma_k = \sum_{n=0}^{\pm\infty} A(|n|a) e^{-in ka}, \quad (48)$$

where n is a non-negative integer and a the lattice constant of the qubit array. Here, J_k and Γ_k can be identified as, respectively, the frequency shift with respect to the isolated qubit frequency ω_{qi} and the single-excitation decay rate of mode k .

Figures 4(a) and (b) display the dependence of the collective excitation spectrum J_k and the decay rate Γ_k on wavevectors within the first Brillouin zone. We observe that the single-excitation modes of the array near the center of the Brillouin zone, i.e., within the green dashed lines in Fig. 4(a), have quasi-momenta that are smaller than the maximum momentum of the spin waves in the magnetic film at the same energy. As a result, these modes can strongly couple to the spin waves of the reservoir, leading to rapid decay characterized by a relaxation rate Γ_k that is larger than that of an isolated qubit, as shown by Fig. 4(b). This behavior is symptomatic of superradiance. On the other hand, modes with quasi-momenta greater than the momentum of the magnon modes are completely decoupled from the magnons. These modes are unable to radiate away energy through the bath, resulting in long-lived, subradiant states. An akin effect has been noted for atoms interacting with light – specifically, spin wavevectors whose magnitudes exceed the dispersion relation of light, i.e., $|k| > \omega/c$ with c being the light speed, have exactly zero decay rate in the limit of an infinite chain [24].

For subradiant states to appear, the spin-wave frequency $\omega_F(k)$ (34) in the magnetic film at certain quasi momenta should be larger than the qubit resonance frequency ω_{qi} , i.e., $\omega_{qi} < \omega_F(k)$. At these wavevectors, the energy emitted from the qubits is not sufficient to create single magnons in the magnetic film. This condition must be satisfied within the boundaries of the first Brillouin zone: $\omega_F(\pi/a) = D(\pi/a)^2 + \Delta_F \geq \omega_{qi}$, which translates into the constraint $a/\lambda \leq \pi$ for the characteristic wavelength λ . The wavelength $\lambda = [D/(\omega_{qi} - \Delta_F)]^{1/2}$ can be enhanced by controlling the detuning $\omega_{qi} - \Delta_F$ via an external magnetic field and by choosing a magnetic bath with high Curie temperature.

In the following, we investigate the properties of the single-excitation sector of a qubit array of finite size. By utilizing the property that the non-Hermitian Hamiltonian \mathcal{H}_{eff} commutes with the particle number operator $\hat{n} = \sum_\alpha \sigma_\alpha^+ \sigma_\alpha^-$, i.e., $\hat{n}\mathcal{H}_{eff} - \mathcal{H}_{eff}\hat{n} = 0$, one can

characterize its eigenstates within each excitation manifold. The non-Hermitian Hamiltonian \mathcal{H}_{eff} is symmetric, i.e., $\mathcal{H}_{eff}^T = \mathcal{H}_{eff}$ (where T denotes the transpose). Thus, its left, $|\psi_n^L\rangle$, and right, $|\psi_n^R\rangle$, eigenstates are related as $|\psi_n^L\rangle \propto (|\psi_n^R\rangle)^*$ and we can diagonalize the non-Hermitian Hamiltonian using its right eigenstates, i.e., $\mathcal{H}_{eff}|\psi_m^R\rangle = E_m|\psi_m^R\rangle$, where $1 \leq m \leq N$. For convenience, we arrange the single-excitation eigenstates in ascending order of decay rate, i.e., $|\psi_1^R\rangle$ and $|\psi_N^R\rangle$ label, respectively, the most subradiant and the most radiant states.

Figure 4(c) show the decay rates of the single-excitation modes of a chain of $N = 40$ solid-state spin defects as function of lattice constant a/λ . As the interqubit distance increases, the effective qubit-qubit dissipative interaction decreases and the collective decay rates approach the spontaneous emission rate of a single atom. Conversely, for smaller lattice constants, one can observe a reduction in the decay rate, which indicates the formation of subradiant states. Remarkably, when the interparticle distance reaches the critical point $a/\lambda = \pi$, the most subradiant decay rate experiences a significant drop, approaching zero as suggested by the infinite array analysis. Figure 4(d) shows the decay rate Γ_1 of the most subradiant state $|\psi_1^R\rangle$ as function of the number N of solid-state spin defects. For an interqubit distance $a/\lambda = 0.1$ the relaxation rate of the most subradiant state approaches quickly zero even for a finite chain.

VI. MULTI-EXCITATION SECTOR

In this section, we explore the ensemble dynamics in the multi-excitation sector, i.e., corresponding to multiple qubits simultaneously initialized into the excited state. This regime is immediately relevant to experimental verifications of our proposed model, as it does not require single-qubit addressability. We show that the collective relaxation rates routinely measured in quantum sensing setups can display clear signatures of cooperative quantum behavior, and we investigate their robustness against experimentally relevant perturbations, i.e., temperature and spatial disorder. Finally, we explore the correlations of the most subradiant two-excitation states.

A. Zero-temperature dynamics

In the multi-excitation sector, the quantum jump terms can not be neglected, and, thus, Eq. (44) has to be solved exactly. We first consider the zero-temperature limit, i.e., $\bar{\Gamma}_{\alpha\beta} = 0$, and solve Eq. (44) numerically using the quantum jump method [86]. We compute the ensemble collective relaxation rate, i.e., $\frac{d}{dt} \sum_{\alpha=1}^N \langle \sigma_\alpha^z \rangle$, which is proportional to the photoluminescence signal that is routinely measured in, e.g., dense NV-center ensembles [14].

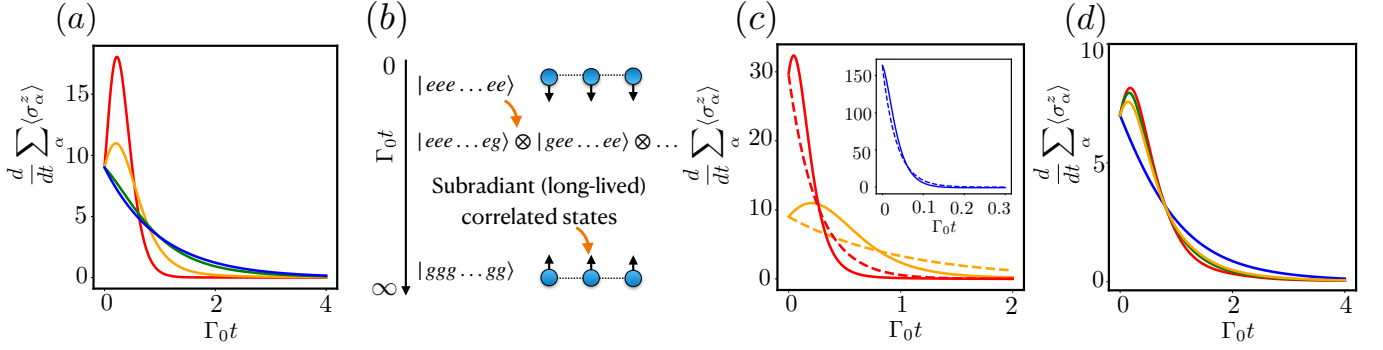


FIG. 5. (a) Zero-temperature collective relaxation rate of an ensemble of $N = 9$ solid-state spin defects initialized in the excited state as a function of time. The red, orange and green lines correspond to arrays with lattice constant $a/\lambda = 0.1, 0.7$ and 2 , respectively. The blue line corresponds to magnon emission rate of a noninteracting ensemble. When the spin defects are placed sufficiently close to each other, the collective emission rate displays a superradiant burst followed by a subradiant tail. (b) The ensemble relaxation dynamics goes through the “Dicke ladder”, i.e., the energy levels of the many-body system can be organized into a ladder-like structure, where each rung corresponds to a given number of excitations. Superradiant states decay toward subradiant states, which can exhibit strong quantum correlations and entanglement. (c) Collective relaxation rate of an ensemble of $N = 9$ solid-state spin defects initialized in the excited state as a function of time at $T = 10$ mK (orange curves), $T = 100$ mK (red curves) and $T = 300$ mK (blue curves in the inset). The solid and dashed lines corresponds to the relaxation rates calculated for $a/\lambda = 0.5$ and $\lambda \rightarrow \infty$ (i.e., a noninteracting array), respectively. (d) Zero-temperature collective relaxation rate of an ensemble of $N = 7$ solid-state spin defects initialized in the excited state as a function of time for $a/\lambda = 0.5$ and disorder strength $\xi = 0$ (red line), $\xi = 5$ (green line) and $\xi = 10$ (yellow line). The blue line corresponds to a noninteracting ensemble. (a,c,d) The time t is units of the relaxation time Γ_0 of an array of N noninteracting spin defects. In each figure, the parameters used are for an ensemble of NV-center spins interacting via a YIG thin film.

Figure 5(a) displays the time evolution of the collective relaxation rate of an array of $N = 9$ solid-state spin defects initialized in the fully excited state. When the inter-qubit distance is smaller than the characteristic wavelength, i.e., $a < \lambda$, the emission rates of the correlated ensemble (red and yellow orange lines) are critically different from the uncorrelated case (blue line). At short times, the relaxation rate of the correlated ensemble displays a burst, in contrast to the exponential decay of the uncorrelated ensemble. Comparing the case of $a = 0.7\lambda$ (orange curve) and $a = 0.1\lambda$ (red curve), we find that the intensity of the burst is enhanced for smaller inter-qubit distances, while the time needed to reach the superradiance peak becomes shorter. The dynamics of the many-body density matrix can be understood in terms of the “Dicke ladder” shown in Fig. 5(b). The superradiant speed up of the collective relaxation, which removes the excess energy from the ensemble in a semiclassical fashion, is followed by a slower transient dynamics of subradiant modes that can exhibit strong quantum correlations and entanglement [30, 87, 88].

Our results suggest that signatures of superradiance and subradiance are experimentally detectable even for a small, i.e., $N = 9$, ensemble of correlated solid-state spin defects, as long as the ensemble relaxation rate is larger than the intrinsic relaxation time of solid-state spin defects. Since the latter can reach even minutes at very low temperatures [89], the strength $\nu \propto D^{-2}$ of the interactions between a spin defect and a ferromagnetic bath does not have to be particularly large, which leaves room for maximizing the characteristic lengthscale

$\lambda \propto D^{1/2}$ via a stiffer magnetic bath. Importantly, one can tune the strength of quantum correlations via an external magnetic field, which allows to probe distinct coupling regimes within one sample.

B. Thermal fluctuations and spatial disorder

In our setup, the impact of finite temperatures opens up a line of investigation that has not been systematically explored at light-matter interfaces. At finite temperatures, a magnetic bath at thermal equilibrium is populated according to the Bose-Einstein distribution, and thermal magnons can interact with the qubit ensemble via the correlated absorption term $\tilde{\Gamma}_{\alpha\beta}$ in Eq. (44).

We explore the impact of thermal fluctuations on quantum cooperativity by numerically simulating Eq. (44) at finite temperature T . Figure 5(c) shows that cooperative behavior is suppressed with increasing temperature, as one would naturally expect since the pumping term counterbalances the collective decay through the Dicke ladder (cf. Fig. 5) which is responsible for superradiance. However, for temperatures of the order $T \sim k_B/\omega_{qi}$, i.e., $T = 100$ mK, which can be feasibly accessed experimentally, superradiant and subradiant deviations from the exponential relaxation of an isolated ensemble (red line) are still clearly visible. Interestingly, when the temperature is finite but not high enough to suppress cooperative effects, the rate of the quantum many-body dynamics increases, i.e., the superradiant burst is reached at shorter times. This occurs as the temperature increases the dis-

sipative correlations according to Eq. (42), which leads to stimulated emission and a consequent speed-up in the collective relaxation dynamics.

Although the fabrication efficiency of ordered arrays of solid-state spin defects is continuously improving [9, 90, 91] and solid-state spin defects in hexagonal boron nitride (hBN) can be deterministically generated [92], spatial disorder in the qubit positions is still likely to play a role in the experimental realizations of our proposal. In order to model spatial disorder we consider an array with random variations in the individual position r_α of each qubit, i.e., $r_\alpha \rightarrow r_\alpha + \delta r_\alpha$. We treat the positional displacement δr_α as a random variable uniformly distributed within the interval $\delta r_\alpha \in (-a\xi/2, a\xi/2)$ where ξ quantifies the strength of disorder. We consider $\xi = 5, 10$ and for each degree of disorder we report an average of the collective relaxation rate over $N_d = 10$ realizations of qubit positions. Figure 5(d) shows that signatures of cooperative behavior are still clearly visible for large disorder strength ξ , demonstrating the robustness of the system against spatial imperfections. Our findings align with experimental observations of cooperative dynamics in dense disordered ensembles of qubits [93–98].

It is also important to note that our results are constrained to the relatively small number N of qubits that quantum many-body simulations can numerically tackle. Since these phenomena are cooperative, the intensity of both subradiant and superradiant signals increases with the number of solid-state defects, which might further relax the temperature and disorder constraints.

C. Correlations

While the long-time collective relaxation dynamics is dominated by the most populated single-excitation subradiant states, two-excitation subradiant states have been recently scrutinized in waveguides as they offer a window into the nontrivial correlations of the many-body quantum dynamics. In 1d arrays of atomic emitters interacting via a photonic reservoir, the most subradiant two-excitation states can be built from fermionic combinations of single-excitation eigenstates [24, 99–101]. This fermionization is intimately connected with the finite group velocity that the qubit array band structure acquires when the real frequency shift (47) is nonzero, i.e., $J_k \neq 0$ [100]. A recent work has confirmed that for a flat band structure, i.e., $J_k = 0$, the subradiant two-excitation states do not display fermionic correlations, but behave as quasilocated dark states with enhanced lifetime [102]. Our 2d reservoir, however, does not allow to access this regime: while we can modulate the characteristic wavelength λ via an external magnetic field, Fig. 3(b) shows that it is not possible to identify a lattice constant a/λ for which the frequency shift J_k vanishes at every order of neighboring interactions. Thus, in our setup both coherent and dissipative interactions always compete to shape novel dynamical many-body quantum

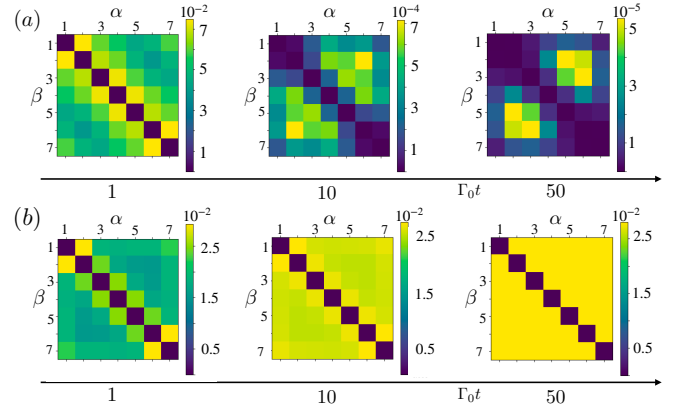


FIG. 6. Second-order correlation function $c_{\alpha\beta}$ at selected times for $T = 0$ (a) and $T = 100$ mK (b). In each figure, the parameters used are for an ensemble of NV-center spins interacting via a YIG thin film.

states.

In order to investigate the multi-excitation correlations of our model, we compute numerically the second-order correlation function $c_{\alpha\beta} = \langle \sigma_\alpha^+ \sigma_\beta^+ \sigma_\beta^- \sigma_\alpha^- \rangle$ from Eq. (44). In the simulation, initially all qubits are in the excited state. Subsequently, the system evolves in accordance with the master equation (44) and transitions into a lower-excitation regime. Figure 6(a) shows the time evolution of the correlation function $c_{\alpha\beta}$ at zero temperature for $a/\lambda = 0.5$. Physically, it can be interpreted as the probability of the solid-state spin defects α and β to be excited at a given time. When $\alpha = \beta$, the correlation function vanishes, i.e., $c_{\alpha\alpha} = 0$, since a single spin-1/2 qubit can not be excited twice. For $\alpha \neq \beta$, the correlations display a fermionic behavior analogous to one found at light-matter interfaces [24, 99–101], with excitations displaying anti-bunching as time grows (cf. second and third upper panel of Fig. 6). Our finding further suggests that the fermionization of subradiant two-excitation states might be a generic feature of dispersive, i.e., $J_k \neq 0$, many-body quantum systems, independently of the specific form of bath-qubit interactions. We then investigate the role of the thermal fluctuations on the quantum correlations by simulating Eq. (44) at finite temperatures. Figure 6(b) shows that, as one might intuitively expect, the thermal fluctuations eventually disrupt fermionic correlations between multi-excited states.

VII. DISCUSSION AND CONCLUSIONS

In this work, we have introduced a general framework for exploring the quantum many-body dynamics of an array of solid-state spin defects interacting dissipatively via the magnetic field fluctuations of a solid-state reservoir. We have then specialized our findings to a ferromagnetic bath and shown that signatures of cooperative quantum dynamics, i.e., superradiant and subradiant states, can

be engineered within experimentally accessible regimes. In particular, we have addressed the robustness of these phenomena to spatial disorder and thermal fluctuations as present in any practical implementation.

Due to the diverse and tunable properties of magnetic systems, our work unlocks an unprecedented versatility in reservoir engineering that future investigations should systematically address to identify the optimal bath and experimental regimes for generating robust, long-range dissipative correlations between solid-state spin defects. The dynamics of magnons can be guided through the influence of diverse non-equilibrium agents, such as currents and gradients in chemical potential, thus unlocking the potential for cooperative phenomena in the presence of controllable far-from-equilibrium baths. This capability remains beyond the grasp of quantum optics, where the environment assumes a passive role as an inert mediator of interactions. Furthermore, our findings introduce an entirely novel domain for non-unitary many-body dynamics amid structured dissipation. In contrast to atom-light matter interfaces, where non-local emission represents the only pathway to produce correlated decoherence, an ensemble of NV centers can experience the combined effects of correlated absorption, emission, and dephasing. This scenario raises numerous captivating inquiries, spanning from the dynamical control of correlations spreading to the real-time formation of entanglement. For instance, our experimental setup naturally lends itself to investigating the prerequisites for establishing many-particle entanglement in the presence of spatially non-local dephasing — a captivating and counter-intuitive avenue hitherto explored predominantly in systems comprising only a few spins and existing primarily at the theoretical level.

Within the horizon of readily attainable goals, achieving collective entanglement, such as spin squeezing, within our hybrid solid-state platform emerges as merely the initial stride toward the convergence of spintronics

and quantum optics into a common research arena. We regard the findings in this manuscript as a potential foundational cornerstone for embarking on this trajectory.

VIII. ACKNOWLEDGEMENTS

The authors thank Y. Tserkovnyak, K. Holczer, and C. Du for helpful discussions and O. Chelpanova for support with the numerical simulations. X. Li was supported by the National Science Foundation under Grant No. NSF DMR-2144086. B. Flebus acknowledges support from DOE under Grant No. DE-SC0024090. D.E. Chang acknowledges support from the European Union, under European Research Council grant agreement No 101002107 (NEWSPIN); the Government of Spain under the Severo Ochoa Grant CEX2019-000910-S [MCIN/AEI/10.13039/501100011033]; QuantERA II project QuSiED, co-funded by the European Union Horizon 2020 research and innovation programme (No 101017733) and the Government of Spain (European Union NextGenerationEU/PRTR PCI2022-132945 funded by MCIN/AEI/10.13039/501100011033); Generalitat de Catalunya (CERCA program and AGAUR Project No. 2021 SGR 01442); Fundació Cellex, and Fundació Mir-Puig. J. Marino acknowledges support by the Deutsche Forschungsgemeinschaft (DFG, German Research Foundation) – Project-ID 429529648 – TRR 306 QuCoLiMa (“Quantum Cooperativity of Light and Matter”), by the Dynamics and Topology Centre funded by the State of Rhineland Palatinate, and by the QuantERA II Programme that has received funding from the European Union’s Horizon 2020 research and innovation programme under Grant Agreement No 101017733 (‘QuSiED’) and by the DFG (project number 499037529).

-
- [1] I. H. Deutsch, PRX Quantum **1**, 020101 (2020).
 - [2] H. J. Kimble, Nature **453**, 1023 (2008).
 - [3] I. Buluta and F. Nori, Science **326**, 108 (2009).
 - [4] C. L. Degen, F. Reinhard, and P. Cappellaro, Reviews of modern physics **89**, 035002 (2017).
 - [5] M. H. Devoret, A. Wallraff, and J. M. Martinis, arXiv preprint cond-mat/0411174 (2004).
 - [6] M. Kjaergaard, M. E. Schwartz, J. Braumüller, P. Krantz, J. I.-J. Wang, S. Gustavsson, and W. D. Oliver, Annual Review of Condensed Matter Physics **11**, 369 (2020).
 - [7] R. Blatt and C. F. Roos, Nature Physics **8**, 277 (2012).
 - [8] C. D. Bruzewicz, J. Chiaverini, R. McConnell, and J. M. Sage, Applied Physics Reviews **6** (2019).
 - [9] G. Wolfowicz, F. J. Heremans, C. P. Anderson, S. Kanai, H. Seo, A. Gali, G. Galli, and D. D. Awschalom, Nature Reviews Materials **6**, 906 (2021).
 - [10] F. Dolde, I. Jakobi, B. Naydenov, N. Zhao, S. Pezzagna, C. Trautmann, J. Meijer, P. Neumann, F. Jelezko, and J. Wrachtrup, Nature Physics **9**, 139 (2013).
 - [11] A. Bermudez, F. Jelezko, M. B. Plenio, and A. Retzker, Physical review letters **107**, 150503 (2011).
 - [12] T. Gaebel, M. Domhan, I. Popa, C. Wittmann, P. Neumann, F. Jelezko, J. R. Rabreau, N. Stavrias, A. D. Greentree, S. Prawer, *et al.*, Nature Physics **2**, 408 (2006).
 - [13] B. Flebus, Physical Review B **100**, 064410 (2019).
 - [14] F. Casola, T. Van Der Sar, and A. Yacoby, Nature Reviews Materials **3**, 1 (2018).
 - [15] B. Flebus, H. Ochoa, P. Upadhyaya, and Y. Tserkovnyak, Physical Review B **98**, 180409 (2018).
 - [16] B. Flebus and Y. Tserkovnyak, Physical Review Letters **121**, 187204 (2018).
 - [17] H. Wang, S. Zhang, N. J. McLaughlin, B. Flebus, M. Huang, Y. Xiao, C. Liu, M. Wu, E. E. Fullerton, Y. Tserkovnyak, *et al.*, Science advances **8**, eabg8562 (2022).
 - [18] T. Van der Sar, F. Casola, R. Walsworth, and A. Yacoby, Nature communications **6**, 1 (2015).
 - [19] C. Du, T. Van der Sar, T. X. Zhou, P. Upadhyaya, F. Casola, H. Zhang, M. C. Onbasli, C. A. Ross, R. L. Walsworth, Y. Tserkovnyak, *et al.*, Science **357**, 195 (2017).
 - [20] L. Trifunovic, F. L. Pedrocchi, and D. Loss, Physical review X **3**, 041023 (2013).
 - [21] P. Andrich, C. F. de las Casas, X. Liu, H. L. Bretscher, J. R. Berman, F. J. Heremans, P. F. Nealey, and D. D. Awschalom, npj Quantum Information **3**, 1 (2017).
 - [22] B. Flebus and Y. Tserkovnyak, Physical Review B **99**, 140403 (2019).
 - [23] M. Fukami, D. R. Candido, D. D. Awschalom, and M. E. Flatté, PRX Quantum **2**, 040314 (2021).
 - [24] A. Asenjo-Garcia, M. Moreno-Cardoner, A. Albrecht, H. Kimble, and D. E. Chang, Physical Review X **7**, 031024 (2017).
 - [25] M. Reitz, C. Sommer, and C. Genes, PRX Quantum **3**, 010201 (2022).
 - [26] D. E. Chang, V. Vuletić, and M. D. Lukin, Nature Photonics **8**, 685 (2014).
 - [27] A. Sipahigil, R. E. Evans, D. D. Sukachev, M. J. Burek, J. Borregaard, M. K. Bhaskar, C. T. Nguyen, J. L. Pacheco, H. A. Atikian, C. Meuwly, *et al.*, Science **354**, 847 (2016).
 - [28] D. Chang, J. Douglas, A. González-Tudela, C.-L. Hung, and H. Kimble, Reviews of Modern Physics **90**, 031002 (2018).
 - [29] V. A. Pivovarov, A. S. Sheremet, L. V. Gerasimov, J. Laurat, and D. V. Kupriyanov, Physical Review A **101**, 053858 (2020).
 - [30] A. Asenjo-Garcia, M. Moreno-Cardoner, A. Albrecht, H. J. Kimble, and D. E. Chang, Phys. Rev. X **7**, 031024 (2017).
 - [31] G. Facchinetti, S. D. Jenkins, and J. Ruostekoski, Physical review letters **117**, 243601 (2016).
 - [32] E. Shahmoon, M. D. Lukin, and S. F. Yelin, Physical Review A **101**, 063833 (2020).
 - [33] R. J. Bettles, S. A. Gardiner, and C. S. Adams, Physical Review A **94**, 043844 (2016).
 - [34] D. Kornovan, A. Sheremet, and M. Petrov, Physical Review B **94**, 245416 (2016).
 - [35] R. Sutherland and F. Robicheaux, Physical Review A **94**, 013847 (2016).
 - [36] S. D. Jenkins and J. Ruostekoski, Physical Review A **86**, 031602 (2012).
 - [37] E. Shahmoon, D. S. Wild, M. D. Lukin, and S. F. Yelin, Physical review letters **118**, 113601 (2017).
 - [38] J. Marino, Physical Review Letters **129**, 050603 (2022).
 - [39] Physical Review B **105**, 184305 (2022).
 - [40] R. H. Dicke, Physical review **93**, 99 (1954).
 - [41] M. Gross and S. Haroche, Physics reports **93**, 301 (1982).
 - [42] D. Meiser, J. Ye, D. Carlson, and M. Holland, Physical review letters **102**, 163601 (2009).
 - [43] J. G. Bohnet, Z. Chen, J. M. Weiner, D. Meiser, M. J. Holland, and J. K. Thompson, Nature **484**, 78 (2012).
 - [44] L. Ostermann, H. Ritsch, and C. Genes, Physical review letters **111**, 123601 (2013).
 - [45] M. Manzoni, M. Moreno-Cardoner, A. Asenjo-Garcia, J. V. Porto, A. V. Gorshkov, and D. Chang, New journal of physics **20**, 083048 (2018).
 - [46] F. Verstraete, M. M. Wolf, and J. Ignacio Cirac, Nature physics **5**, 633 (2009).
 - [47] D. E. Chang, J. S. Douglas, A. González-Tudela, C.-L. Hung, and H. J. Kimble, Rev. Mod. Phys. **90**, 031002 (2018).
 - [48] J. C. Slonczewski, Journal of Magnetism and Magnetic Materials **159**, L1 (1996).
 - [49] J. Slonczewski, Journal of Magnetism and Magnetic Materials **195**, L261 (1999).
 - [50] L. Berger, Physical Review B **54**, 9353 (1996).
 - [51] S. Takahashi and S. Maekawa, Science and Technology of Advanced Materials **9**, 014105 (2008).

- [52] J. Fransson, J. Ren, and J.-X. Zhu, *Physical Review Letters* **113**, 257201 (2014).
- [53] L. J. Cornelissen, K. J. Peters, G. E. Bauer, R. Duine, and B. J. van Wees, *Physical Review B* **94**, 014412 (2016).
- [54] K.-I. Uchida, S. Takahashi, K. Harii, J. Ieda, W. Koshibae, K. Ando, S. Maekawa, and E. Saitoh, *nature* **455**, 778 (2008).
- [55] A. Barman, G. Gubbiotti, S. Ladak, A. O. Adeyeye, M. Krawczyk, J. Gräfe, C. Adelmann, S. Cotozana, A. Naeemi, V. I. Vasyuchka, *et al.*, *Journal of Physics: Condensed Matter* **33**, 413001 (2021).
- [56] A. Periwai, E. S. Cooper, P. Kunkel, J. F. Wienand, E. J. Davis, and M. Schleier-Smith, *Nature* **600**, 630 (2021).
- [57] C.-L. Hung, A. González-Tudela, J. I. Cirac, and H. Kimble, *Proceedings of the National Academy of Sciences* **113**, E4946 (2016).
- [58] J. Zou, S. Zhang, and Y. Tserkovnyak, *Physical Review B* **106**, L180406 (2022).
- [59] H.-P. Breuer, F. Petruccione, *et al.*, *The theory of open quantum systems* (Oxford University Press on Demand, 2002).
- [60] U. Weiss, *Quantum dissipative systems* (World Scientific, 2012).
- [61] C. Gardiner, P. Zoller, and P. Zoller, *Quantum noise: a handbook of Markovian and non-Markovian quantum stochastic methods with applications to quantum optics* (Springer Science & Business Media, 2004).
- [62] A. Rivas and S. F. Huelga, *Open quantum systems*, Vol. 10 (Springer, 2012).
- [63] E. B. Davies, *Communications in mathematical Physics* **39**, 91 (1974).
- [64] V. Gorini, A. Frigerio, M. Verri, A. Kossakowski, and E. Sudarshan, *Reports on mathematical physics* **13**, 149 (1978).
- [65] A.-P. Jauho *et al.*, *Quantum kinetics in transport and optics of semiconductors*, Vol. 2 (Springer).
- [66] S. Diehl, A. Micheli, A. Kantian, B. Kraus, H. Büchler, and P. Zoller, *Nature Physics* **4**, 878 (2008).
- [67] Even when two NV centers have been recently used to probe spatiotemporal correlations of a classical signal, they were operated essentially as two independent qubit sensors [103].
- [68] S. Zhang and Y. Tserkovnyak, *Physical Review B* **106**, L081122 (2022).
- [69] K. Y. Guslienko and A. N. Slavin, *Journal of magnetism and magnetic materials* **323**, 2418 (2011).
- [70] B. Flebus, *Journal of Applied Physics* **129** (2021).
- [71] R. Kubo, *Reports on progress in physics* **29**, 255 (1966).
- [72] L. Landau and E. Lifshitz, in *Perspectives in Theoretical Physics* (Elsevier, 1992) pp. 51–65.
- [73] L. P. Kadanoff and P. C. Martin, *Annals of Physics* **24**, 419 (1963).
- [74] H. Fang, S. Zhang, and Y. Tserkovnyak, *Physical Review B* **105**, 184406 (2022).
- [75] K. Seetharam, A. Lerose, R. Fazio, and J. Marino, *Physical Review Research* **4**, 013089 (2022).
- [76] H. M. Hurst and B. Flebus, *Journal of Applied Physics* **132**, 220902 (2022).
- [77] K. Deng and B. Flebus, *Physical Review B* **105**, L180406 (2022).
- [78] X. Li, M. A. Begaowe, S. Zhang, and B. Flebus, *arXiv preprint arXiv:2307.15792* (2023).
- [79] P. M. Gunnink, B. Flebus, H. M. Hurst, and R. A. Duine, *Physical Review B* **105**, 104433 (2022).
- [80] S. Kamboj, R. A. Duine, B. Flebus, and H. M. Hurst, *arXiv preprint arXiv:2307.13876* (2023).
- [81] K. Deng, X. Li, and B. Flebus, *Physical Review B* **107**, L100402 (2023).
- [82] J. Lee, T. Kottos, and B. Shapiro, *Physical Review B* **91**, 094416 (2015).
- [83] H. Liu, D. Sun, C. Zhang, M. Groesbeck, R. Mclaughlin, and Z. V. Vardeny, *Science advances* **5**, eaax9144 (2019).
- [84] X. Li, K. Deng, and B. Flebus, *Physical Review B* **106**, 214432 (2022).
- [85] F. Minganti, A. Miranowicz, R. W. Chhajlany, and F. Nori, *Physical Review A* **100**, 062131 (2019).
- [86] J. R. Johansson, P. D. Nation, and F. Nori, *Computer Physics Communications* **183**, 1760 (2012).
- [87] S. J. Masson, I. Ferrier-Barbut, L. A. Orozco, A. Browaeys, and A. Asenjo-Garcia, *Physical review letters* **125**, 263601 (2020).
- [88] J. Rui, D. Wei, A. Rubio-Abadal, S. Hollerith, J. Zeiher, D. M. Stamper-Kurn, C. Gross, and I. Bloch, *Nature* **583**, 369 (2020).
- [89] A. Jarmola, V. Acosta, K. Jensen, S. Chemerisov, and D. Budker, *Physical review letters* **108**, 197601 (2012).
- [90] P. Spinicelli, A. Dréau, L. Rondin, F. Silva, J. Achard, S. Xavier, S. Bansropun, T. Debuisschert, S. Pezzagna, J. Meijer, *et al.*, *New Journal of Physics* **13**, 025014 (2011).
- [91] A. V. Tsukanov, I. Y. Kateev, and A. A. Orlikovsky, in *International Conference Micro-and Nano-Electronics 2012*, Vol. 8700 (SPIE, 2013) pp. 453–465.
- [92] W. Liu, N.-J. Guo, S. Yu, Y. Meng, Z.-P. Li, Y.-Z. Yang, Z.-A. Wang, X.-D. Zeng, L.-K. Xie, Q. Li, *et al.*, *Materials for Quantum Technology* **2**, 032002 (2022).
- [93] C. Bradac, M. T. Johnsson, M. v. Breugel, B. Q. Baragiola, R. Martin, M. L. Juan, G. K. Brennen, and T. Volz, *Nature communications* **8**, 1205 (2017).
- [94] S. Inouye, A. Chikkatur, D. Stamper-Kurn, J. Stenger, D. Pritchard, and W. Ketterle, *Science* **285**, 571 (1999).
- [95] G. Ferioli, A. Glicenstein, F. Robicheaux, R. Sutherland, A. Browaeys, and I. Ferrier-Barbut, *Physical Review Letters* **127**, 243602 (2021).
- [96] G. Rainò, M. A. Becker, M. I. Bodnarchuk, R. F. Mahrt, M. V. Kovalenko, and T. Stöferle, *Nature* **563**, 671 (2018).
- [97] M. Scheibner, T. Schmidt, L. Worschech, A. Forchel, G. Bacher, T. Passow, and D. Hommel, *Nature Physics* **3**, 106 (2007).
- [98] S. Cardenas-Lopez, S. J. Masson, Z. Zager, and A. Asenjo-Garcia, *Physical Review Letters* **131**, 033605 (2023).
- [99] L. Henriët, J. S. Douglas, D. E. Chang, and A. Albrecht, *Physical Review A* **99**, 023802 (2019).
- [100] Y.-X. Zhang and K. Mølmer, *Physical Review Letters* **128**, 093602 (2022).
- [101] A. Albrecht, L. Henriët, A. Asenjo-Garcia, P. B. Dieterle, O. Painter, and D. E. Chang, *New Journal of Physics* **21**, 025003 (2019).

- [102] R. Holzinger, R. Gutiérrez-Jáuregui, T. Hönigl-Decrinis, G. Kirchmair, A. Asenjo-Garcia, and H. Ritsch, *Physical Review Letters* **129**, 253601 (2022).
- [103] J. Rovny, Z. Yuan, M. Fitzpatrick, A. I. Abdalla, L. Futamura, C. Fox, M. C. Cambria, S. Kolkowitz, and N. P. de Leon, *Science* **378**, 1301 (2022).